Inhibited coarsening of a sprayformed and extruded hypereutectic aluminium-silicon alloy in the semi-solid state

S.C. Hogg and H.V. Atkinson

At the time the work was carried out S.C. Hogg and H.V. Atkinson were in the Department of Engineering Materials, The University of Sheffield, Mappin Street, Sheffield, S1 3JD. Dr. Hogg is now in the Department of Materials, University of Oxford, Parks Road, Oxford, OX1 3PH, and Prof. Atkinson is in the Department of Engineering, University of Leicester, University Rd., Leicester, LE1 7RH, UK.

Abstract

The microstructural evolution of a sprayformed and extruded hypereutectic aluminium-30% silicon-5% copper-2% magnesium alloy heated into the semi-solid state has been investigated. Liquid is formed initially by a quaternary eutectic reaction and then by a ternary melt reaction. These reactions occur relatively quickly. However, the binary Al-Si eutectic melt reaction takes a significant time – around several hours depending on the temperature. The coarsening rate constants (K) for the growth of the silicon particles are approximately 3 to 4 orders of magnitude lower than those for the majority of metal sprayformed alloys. This may be associated with difficulties in addition or removal of atoms from the low index silicon facets. Where growth does occur, agglomeration of silicon particles may play a large role, especially at higher liquid contents. Electron backscatter diffraction (EBSD) gives evidence of agglomeration, and furthermore shows that high angle silicon-silicon boundaries are not wetted with liquid.

1 Introduction.

Hypereutectic aluminium-silicon alloys, with silicon contents well above the eutectic composition (12.2 wt.% Si), exhibit desirable physical properties such as high specific stiffness, good wear resistance, low coefficient of thermal expansion, and low density [1]. This makes these alloys interesting for many applications, not least in the automotive and aerospace industries. However, due to the steepness of the liquidus on the silicon-rich side of the eutectic, and the large latent heat associated with silicon freezing, the silicon precipitates slowly as large (up to several mm diameter), angular crystals. This has deleterious effects on the mechanical properties, especially the fracture toughness, and thus silicon contents are generally accepted to be limited to about 18 wt.% in conventionally cast alloys. A well-established method of refining the primary silicon size in hypereutectic aluminium-silicon alloys is to inoculate the melt with a phosphorus-bearing addition [2,3]. However, due to the wide melting range in the far-hypereutectic region, this is not effective above about 25 wt.% silicon.

An alternative approach to refine the primary silicon particle size in these alloys is sprayforming [4], which results in homogeneous, fine-scale microstructures, with low levels of segregation. Hypereutectic Al-Si alloys manufactured by this route exhibit microstructures that are generally free of eutectic silicon, but rather consist of equiaxed silicon particles approximately 1-10 μm in diameter, embedded in a matrix of α-Al solid solution [5,6]. This non-equilibrium microstructure would not be expected from a thermodynamic point of view for hypereutectic Al-Si alloys. The alloys can be considered to be, in effect, metal matrix composites, with the silicon essentially a particulate reinforcing phase in the metal matrix [7]. A further benefit of the equiaxed nature of sprayformed materials is that they are amenable to shaping by semi-solid processing routes (of which thixoforming is one type). Successful thixoforming requires a specific starting microstructure in the semi-solid state; namely discrete spheroids surrounded by a continuous

liquid film [8]. To obtain this microstructure in a commercially acceptable time frame, liquid has to form easily and be able to wet the majority of grain boundaries present. Under these conditions, enhanced mechanical properties can be obtained relative to die casting, due to the smooth laminar flow of the slurry in the die. This reduces segregation, avoids gas entrapment which causes porosity, and, as the metal flow front is not broken up, oxide entrapment is much reduced. Most commercial thixoforming is carried out at around 0.5 volume fraction liquid, mainly using aluminium alloys (a review of the aluminium alloys used for semi-solid processing has been carried out by Atkinson et al. [9]), although semi-solid processing of magnesium alloys is commercially exploited in the form of thixomoulding [10]. Assuming that the feedstock has been produced correctly and careful control of the heating into the semi-solid region is observed, thixotropic flow is readily achieved.

In the types of alloys used in this study, when the silicon content exceeds approximately 27 wt.%, the silicon in the microstructure exists as a three-dimensional interconnected network [5]. This hinders thixoforming. The network has considerable strength, which along with a high proportion of unwetted grain boundaries, inhibits semi-solid processing, causing liquid segregation and incomplete die filling. The aim of this investigation was to try and understand the evolution of the microstructure (i.e. the kinetics of liquid formation and silicon coarsening) when the material was heated into the semi-solid state and held at temperatures of 550°C, 555°C, 558°C and 562°C, which have already been shown [7] to be suitable for semi-solid processing of these materials. Sprayformed and extruded Al-30Si-5Cu-2Mg alloy (all compositions are given in wt.%) was isothermally annealed in a specially designed induction furnace. For comparison, heat treatments were also performed in the solid state (495°C) for 1, 2, 4 and 8 hours.

2 Experimental method and materials

The Al-Si-Cu-Mg alloy was sprayformed by Osprey Metals Ltd. and extruded at Minalex at 330°C. This was carried out to reduce the cross-section of the alloy to a more suitable size.

Extrusion of the sprayformed billets proved difficult; at the maximum force available the extrusion speed was approximately 0.07mm/s. The final diameter of the bar was 72mm, with the extrusion ratio approximately 4.5. The actual composition was 32.6 Si, 4.52 Cu, 1.67 Mg (wt.%). The residual Fe content was 0.18 wt.%. Isothermal heat-treatments were performed on cylindrical samples (12.5mm in diameter and 40mm in height) using a small 5kW radio frequency (approximately 450kHz) induction furnace. A Eurotherm 2404 P.I.D. (Proportional, Integral, Derivative) controller was interfaced to the induction heater to maintain close temperature control (to within $\pm$0.5˚C). Although the temperatures selected for the isothermal annealing treatments are close to each other, the consistent differences in behaviour between the different temperatures, which will be demonstrated below, provide evidence that the temperature control does occur to within these limits. The samples were held horizontally inside a silica tube, within the induction coil, on a small silica boat to position them centrally in the coil. Quenching, to arrest microstructural development, was carried out by pouring water in via a side arm. Samples were isothermally heat-treated at 495°C for 1, 2, 4, and 8 hours, and at temperatures suitable for thixoforming of 550, 555, 558 and 562°C for 5 minutes to 8 hours. The 495°C heat treatment is approximately 10°C below the solidus temperature. The other temperatures are in the solid-plus-liquid region, but, as will be shown later, the liquid fraction evolved gradually with time, and so a unique fraction solid cannot be attributed to each temperature. After heat treatment and quenching, sections were prepared for metallography in the usual manner. Optical microscopy was performed on unetched samples using an Olympus Vanox microscope and images captured using a JVC KK-F55B CCD camera driven by Neotech Image Grabber PCI software. Image analysis was carried out using commercially available image analysis software. Differential Scanning Calorimetry (DSC) was carried out using a TA Instruments 910 with carbon pans (as the sample reacted with the standard aluminium pans), calibrated by melting indium and lead at the relevant heating rate. The heating rate was 40 K/min. Electron backscatter

diffraction (carried out at Oxford University Materials Department) was performed using a JEOL 6500 FEG-SEM with TSL OIM data collection and analysis software.

3 Results and discussion

3.1 Differential Scanning Calorimetry (DSC)

Figure 1 shows the DSC trace obtained on heating to 562°C, using a heating rate of 40°C /minute. This was the fastest heating rate the machine was calibrated for, and of a similar rate to that experienced during heating in the induction furnace. The endotherm beginning at around 508°C probably corresponds to the quaternary Al-Si-Al_2Cu-$Al_5Si_6Cu_2Mg_8$ (Al-Si-θ-Q) eutectic. This is in reasonable agreement with literature values [11]. There is a progressive decline in the base line after the first endotherm, most likely resulting from dissolution of silicon and other elements into the aluminium as the solid-solubility increases with temperature. The inflection which is arrowed at approximately 525°C is consistent with the Al-Si-Al_2Cu (Al-Si-θ) ternary eutectic reaction [11]. The endotherm at approximately 540-545°C probably corresponds to the Al-Q binary (at 540°C) or Al-θ binary (at 548°C). A further endotherm is evident at around 560°C, which may be due to the binary Al-Si eutectic reaction. It should be noted that, as will be shown below, the binary eutectic reaction has very sluggish kinetics, and this will affect the DSC results.

3.2 Microstructural evolution

Figures 2 to 5 show the chronological development of the alloy microstructure on heat treatment at 550°C, 555°C, 558°C and 562°C for 5, 15, 30, 60, 120 and 480 minutes. The lightest phase is the aluminium-solid solution, the dark grey phase is the silicon, and the mid-grey phase is the quenched liquid. The black regions are not the Mg_2Si phase, but probably regions where the quenched liquid has been pulled out during polishing. Note here that the magnifications are different, especially at the increased temperatures, but micron markers are included.

Figure 2 shows the observed microstructures on isothermal holding for up to 8 hours at 550°C. Here it is apparent that the silicon is coarsening progressively, and that the liquid content is slowly increasing with time at temperature, from approximately 5% to 14% (from image analysis) between the 5 minutes and 8 hours heat treatment. The liquid is not completely surrounding the silicon; there are many grain boundaries not wetted by liquid at all holding times. Figure 6 shows the microstructure of the alloy soaked for 5 minutes and 8 hours at 550°C at higher magnification to confirm this observation. It is clear that after 8 hours the aluminium spheroids have remained intact and there is only a small amount of quenched liquid present, indicating that the binary eutectic reaction has not commenced to any significant degree.

Figure 3 shows the observed microstructures on isothermal holding for up to 8 hours at 555°C. Between 5 minutes and 60 minutes (same magnification), the silicon is coarsening progressively and the liquid contents are similar (6 and 9% respectively). However, there is a large increase in the liquid content between 5 minutes and 8 hours – Figure 7. There is evidence of fine aluminium dendrites from the quenched liquid at a holding time of 8 hours suggesting the onset of the binary eutectic reaction. This variation in liquid content with time is greater as the temperature is increased, and is quantified in Table 1. The liquid content from image analysis was higher as the temperature increased, but remained reasonably constant between 5 minutes and 60 minutes at each temperature. At 120 minutes and above, for the heat treatments at 555, 558 and 562°C, the liquid content increased considerably with time.

Figure 8 illustrates the observed microstructures after holding for 8 hours at 558 and 562°C respectively. The microstructure consists of silicon + quenched liquid. Especially apparent at higher temperatures and times is agglomeration of the silicon, evidenced by a ‘branched’ or non-equiaxed silicon morphology. Furthermore, entrapped liquid within the particles suggests that agglomeration of the silicon has taken place.

3.3 Rate constants for the coarsening of the silicon

Figure 9 graphically illustrates the coarsening data. For the shorter times and lower temperatures, thousands of particles have been analysed, for the higher times and longer temperatures, hundreds. The 95% confidence limits are shown. It is clear that, for a given time, the average silicon size generally becomes larger as the isothermal holding temperature is increased. A steady reduction in the rate of increase with time was observed in the samples held at 550°C. At 555, 558 and 562°C, the particle growth rate declined between 5 minutes and 60 minutes (figure 9 insert). However, the growth rate increased between 60 minutes and 120 minutes, decreased between 120 and 240 minutes and increased between 240 and 480 minutes. The erratic nature of the variation in rate of particle size increase is attributed to the differences in liquid contents with time (Table 1). Table 1 indicates that at 550°C the liquid content increases only slightly with time, whereas the higher annealing temperatures produce appreciably increased liquid with time.

To compare with data in the literature we need to obtain a coarsening rate constant. Experimentally observed coarsening in the semi-solid state (even at high solid fractions) [12], is usually treated in terms of cubic kinetics (diffusion controlled coarsening) and this will be assumed to be the case here. Furthermore, a statistical analysis of concurrent diffusion controlled coarsening and grain coalescence [13] has shown that cubic kinetics is still applicable, with the coarsening rates depending on the relative contributions of the two mechanisms.

Figure 10 shows a silicon coarsening plot assuming cubic kinetics, i.e.

$$d^3 = d_o^3 + Kt \qquad (1)$$

where d is the average particle diameter at time t, d_o is the initial average particle diameter and K is the coarsening rate constant. For the higher temperature heat treatments, the data do not lie on a straight line across the entire time range. Table 2 shows the observed semi-solid coarsening

rate constants, K, assuming a linear fit over the entire range of times, with regression coefficients. The coarsening rate constants in the semi-solid state are very sensitive to temperature, with an approximate order of magnitude increase per few °C.

Figure 10 (insert) illustrates a magnification of the cube of the average silicon diameter vs. time between 5 and 60 minutes. For this range of times, the curves exhibit a reasonable fit to the cubic power law model. The coarsening rate constants, $K^{5\text{-}60}$, for heat treatment times between 5 minutes and 60 minutes were obtained from the linear best-fit lines and are also shown in Table 2. $K^{5\text{-}60}$ values increase by approximately a factor of five between the 550°C and 562°C annealing temperatures. It is evident from the microstructures (Figures 2 – 5) that the liquid content of the samples (Table 1), although higher as the temperature was increased, remained reasonably constant between 5 minutes and 60 minutes. At 120 minutes and above, for the heat treatments at 555, 558 and 562°C, the liquid content increased considerably with time at temperature, consistent with the larger coarsening constant, and large increase in the coarsening constant over the entire range of annealing times.

Typical coarsening rates for various sprayformed metal alloys, including AA2014, Cu-Ti, In-625 [12], UDIMET 720, MAR-M-002 [14] and IN718 [15], are in the region of 1×10^{-16} m^3s^{-1}. This is some orders of magnitude faster than the results of this study, suggesting coarsening of the silicon in this system is inhibited relative to other sprayformed metal systems.

Due to the high fractions of solid present in the semi-solid state in this system, rather than considering the diffusion fields around isolated particles (as in the LSW analysis [16,17]), a modified liquid film migration model [15], which considers migration of the liquid films separating the grains, is used to predict the coarsening coefficient:

$$\bar{r}_t^{-3} - \bar{r}_0^{-3} = \frac{3D\gamma V_m C_l (1 - f_s)}{2(C_l - C_s)RT(1 - f_{so})(f_{so}^{-1/3} - 1)} t, \text{ or } \bar{r}_t^{-3} - \bar{r}_0^{-3} = K't \quad (2)$$

where, $\bar{r}_0$ and $\bar{r}_t$ are the average particle radius initially and at time t respectively, D is the diffusion coefficient, γ is the interfacial free energy in the solid-state, V_m is the molar volume of the coarsening component, C_l and C_s are the concentration of solute in the liquid and solid respectively, f_s is the solid fraction (which in this study varies as a function of time at temperature - Table 1) and f_{so} is the solid fraction where solid-solid contacts occur, i.e. the liquid thickness remains constant, but the area of contact is reduced. R and T have their usual meanings. Note that, to facilitate direct comparison with values in the literature e.g. [12, 15, 18], the experimentally obtained coarsening coefficients (K) were calculated using $\bar{d}_t^3 - \bar{d}_0^3 = Kt$. The predicted K' value in Eq. 2 and below in Eq. 3 are equal to one eighth this value. In the text and in the Tables, all predicted coarsening coefficients are stated in terms of K, i.e. 8K'.

As silicon is essentially pure in the Al-Si system [19], and the concentration of solute in the solid silicon is in effect zero, $(C_l/(C_l-C_s)) \rightarrow 1$, and can therefore be neglected. If we assume that the grain boundaries of silicon are not wet by the liquid, which appears to hold true in this alloy, we can take $f_{so} \sim 0.7$ (the maximum packing for spheres). This model predicts an increase in the coarsening rate with increased liquid content in the high solid fraction regime, where the solid is not separated by continuous liquid films (above ~ 0.7), consistent with observations here.

For fractions of solid that are less than 0.7, i.e. the 120, 240 and 480 minutes treatment at 562°C, and the 480 minutes treatment at 558°C, the silicon particles are not in contact, and the liquid film migration model takes the form [15]:

$$\bar{r}_t^{-3} - \bar{r}_0^{-3} = \frac{3D\gamma V_m C_l t}{2(C_l - C_s)RT(f_s^{-1/3} - 1)} \quad (3)$$

A benefit of using these models is that it allows us to illustrate the effect of liquid fraction on the predicted coarsening coefficient. The data used to predict the coarsening parameter is given in Table 3. The predicted K values in the semi-solid state as a function of temperature and solid fraction, using the relevant model above, along with the fraction solid established using image analysis, are presented in Table 4.

In the semi-solid state, the predicted values are higher than those obtained experimentally, even though the effect of the high fraction of solid has been considered. Initially there is very little liquid, and the coarsening species must be transported through the solid matrix or along grain boundaries (slow diffusion paths relative to diffusion in the liquid), or through any liquid channels that might connect the silicon, and this effect may not be entirely accounted for by the model. Coarsening may be inhibited if there are minority insoluble second phase particles (dispersoids or precipitates) located at grain boundaries, which pin the boundaries and/or the migrating liquid film [12]. These become ineffective as the temperature is increased when they either dissolve, or the liquid film thickness becomes greater than the particle size. This could give rise to the observed increase in K with increased temperature [12, 14] at low fractions of solid. This appears not to be the case in this study, as TEM including EDX of the sprayformed material, failed to reveal the presence of an impurity second phase at grain boundaries within the limit of the elements scanned (Al, Si, Cu and Mg) [21], although aluminium precipitates have been seen at, or close to, silicon-silicon grain boundaries [22]. Additional considerations of sluggish kinetics will be discussed below. The predicted K values vary by less than an order of magnitude across the entire temperature and solid fraction range, rather than by an order of magnitude every few °C as observed experimentally in this study. This will be discussed later in terms of the contribution of agglomeration of the silicon particles to the growth rate.

3.2 Kinetic considerations in connection with silicon surfaces

A possible reason for the slow liquid formation and inhibited coarsening relative to metal systems is given by considering the free energy change consequent with the addition or loss of atoms from a silicon surface. The change in free energy as a monolayer is added or removed from a crystallographically perfect crystal surface can be obtained using the model by Jackson [23]. According to the model, for silicon in contact with molten silicon, the {111} surfaces will be faceted ($\alpha \geq 2$) whereas the other surfaces should be atomically diffuse. For silicon growing from liquid at the eutectic temperature, rather than from its pure melt at approximately 1414°C, the faceting effect is emphasised [24], presumably as the entropy change will be larger for the more ordered silicon atomic array at the lower temperature, and the Al-Si liquid will be more disordered than pure Si liquid. Both the {111} and {100} surfaces should be atomically smooth. The increase in free energy as the {111}, and to a lesser extent the {100}, surfaces proceed from atomically smooth to atomically rough may be the cause of the sluggish kinetics at the solid/liquid interface, and therefore slow coarsening and liquid formation.

3.3 Contribution to growth rate from agglomeration.

At higher temperatures and after long isothermal holding times, where there is a lower fraction of solid, there is evidence that agglomeration of particles plays a role in the growth of the primary silicon. It is evident from the graphs of silicon particle size vs. time that the coarsening rate increases in the low fraction solid regime, e.g. for the alloys heat treated at 558 and 562°C from 120 to 480 minutes. This increased growth rate may be due to growth from agglomeration. Furthermore, the K values increase with increasing temperature (despite greater diffusion distances), which is contrary to the model used here (eqs. 2 and 3) and LSW theory [16,17], but again, consistent with a contribution to particle growth from agglomeration. There is microstructural evidence for agglomeration; the non-equiaxed silicon morphology and increased

entrapped liquid within the primary silicon - Figure 8. Under certain growth conditions (large silicon particle size > 50μm and low undercooling) silicon can adopt a branched morphology, due to dendritic out-growths at corners and edges [25]. To investigate whether the branched morphology of the silicon was due to agglomeration, or due to the growth under the condition described as 3rd stage growth in ref [25], electron backscatter diffraction was performed. Figure 11(a) shows an EBSD pattern image quality map of a typical large silicon particle from the sample heat-treated at 562°C for 2 hrs. Light regions in the map are from regions with few lattice defects. Grain boundaries are regions with a high proportion of defects and show as dark. The variations in the grey-scale in different areas in the particle are a consequence of the different crystal orientations. The particle consists of a large central grain, with several smaller grains contained within it and attached to it. There is evidence of the agglomeration process, with separate grains attached by high angle boundaries (>15°) at the facets, rather than at corners. High angle boundaries are shown as black lines and 59-61° boundaries (corresponding to Σ3 {111} twin boundaries) as light grey lines in Figure 11(b), which is for the same area as 11(a) and indicates regions of high silicon EDS counts as light. The particle exhibits faceting on the {111} planes (planes parallel to Σ3 {111} twin boundaries, marked by thin grey lines in the figure), as predicted by the Jackson model. There is evidence that the growth mechanism (other than agglomeration) is the twin plane re-entrant (TPRE) mechanism [26, 27], with twin grooves and ledges present.

Agglomeration will occur if $\gamma_{gb} \leq 2\gamma_{sl}$, where γ_{gb} and γ_{sl} are the grain boundary energy and solid/liquid interface energy respectively [28]. Dihedral angle studies for liquid eutectic Al-Si against solid silicon-silicon boundaries at 580°C [29] and 577°C [30], revealed the grain boundary energy to be equal to the solid/liquid interface energy, i.e. the dihedral angle was ~120°. Taking the energy of high angle silicon-silicon boundaries to be 1.3-1.37 Jm^{-2}, as obtained from computer simulations of high angle twist boundaries [31, 32], and the solid/liquid

interface energy to be approximately 0.5 Jm^{-2} (calculated from [30], corrected with a liquidus slope of 2350K/atom fraction from [19]), this suggests such boundaries will be wetted by liquid ($\gamma_{gb} > 2\gamma_{sl}$). For agglomeration to occur, these high angle boundaries will need to be favourably orientated to a low energy configuration, or have their energy lowered by some other mechanism. Monte Carlo simulations of a Σ31 {111}-plane boundary predict the energy to be 0.86 Jm^{-2} [31], in which case a single boundary of this geometry will be energetically favoured over two solid-liquid interfaces. In a Σ31 boundary, 1 in 31 of the lattice sites coincide. This is a reasonable approximation to a random boundary [33], i.e. the boundary ceases to exhibit 'special' properties. Therefore, {111} plane high angle boundaries in silicon should all be around this energy. Selected area electron diffraction [11] and EBSD have shown that the silicon in this system exhibits facets extensively on the (low energy [31, 34]) {111} plane (as predicted by the Jackson model mentioned above). A large proportion of agglomeration boundary planes will, therefore, probably be of the {111} type, leading to a high probability that agglomeration will occur. Additionally, there is evidence in the literature of agglomeration of primary silicon particles in Al-Si alloys [35, 36], and that silicon boundaries, generally, have a tendency to adopt special, low energy, geometries [37, 38].

4 Conclusions

The microstructural evolution of a sprayformed and extruded Al-30Si-5Cu-2Mg alloy has been investigated at 495, 550, 555, 558, and 562°C. During isothermal annealing in the semi-solid state, the liquid content generally increased with time, but slowly.

Experimentally obtained K values for the coarsening of silicon, assuming cubic coarsening kinetics, are several orders of magnitude lower than those typically obtained for sprayformed

metal systems. The K values increase with temperature by approximately an order of magnitude per few °C. Apart from the 495°C and 550°C heat treatments, the rate of increase in particle size does not decrease with time, but varies erratically. This is probably due to effects associated with changes in the liquid content with time at temperature.

Predicted values of the coarsening coefficient are considerably higher than those obtained in the semi-solid state. This is probably associated with sluggish kinetics at the solid/liquid interface.

There is an observed acceleration in the coarsening rate at increased fraction liquid, despite increases in diffusion distances. We would argue that the higher growth rate at higher temperatures is associated with agglomeration, and EBSD has revealed that agglomeration of silicon does occur even when the grains are oriented to give high angle boundaries between agglomerated particles. Particles can move more freely within the increased liquid allowing them to minimise their misorientation (if necessary) and collide. Agglomeration may be further encouraged by the faceted nature of the boundaries which may result in lower energy agglomeration boundaries.

Acknowledgements

The authors are grateful to Osprey Metals Ltd. (Neath U.K.) for the supply of the materials. This work was carried out partly under the auspices of the EPSRC IMI project GR/K66611.

References

[1] N. Tenekedjiev and J.E. Gruzleski: A.F.S. Trans., 1989, vol. 97, pp. 127-136

[2] N. Tenekedjiev and J.E. Gruzleski: Cast Metals, 1990, vol. 3, pp. 96-105

[3] W.J. Kyffin, W.M. Rainforth and H. Jones: Mater. Sci. Tech., 2001, vol. 17, pp. 901-905

[4] P.S. Grant: Prog. Mater. Sci., 1995, vol. 39, pp. 497-545

[5] P.J. Ward, H.V. Atkinson, D.H. Kirkwood and C.M. Sellars: Proc. 2nd Int. Conf. on Semi-solid Processing of Alloys and Composites, Editors, pp. S.B. Brown and M.C. Flemings, Cambridge, Massachusetts, USA, 1992, pp. 440-446

[6] E.J. Lavernia and Y. Wu: Spray Atomization and Deposition, John Wiley and Sons, Chichester, 1996

[7] P.J. Ward, H.V. Atkinson, P.R.G. Anderson, L.G. Elias, B. Garcia, L. Kahlen and J.M. Rodriguez-Ibabe: Acta Metall. Mater., 1996, vol. 44, pp. 1717-1727

[8] M.C. Flemings: Met. Trans. A, 1991, vol. 22A, pp. 957-981

[9] H.V. Atkinson, P. Kapranos and D.H. Kirkwood: Proc. 6th Int. Conf. on Semi-solid Processing of Alloys and Composites, eds. G.L. Chiarmetta and M. Rosso, Turin, 2000, pp. 443-450

[10] D. Walukas, S. LeBeau, N. Prewitt and R. Decker: Proc. 6th Int. Conf. on Semi-solid Processing of Alloys and Compsites, eds. G.L. Chiarmetta and M. Rosso, Turin, 2000, pp. 109-114

[11] F. Mondolfo: Aluminium Alloys, Structures and Properties, Butterworth, London, pg. 773, 1976

[12] S. Annavarapu and R.D. Doherty: Acta Metall. Mater., 1995, vol. 43, pp. 3207-3230

[13] S. Takajo, W.A. Kaysser and G. Petzow: Acta Metall. Mater., 1984, vol. 32, pp. 107-113

[14] R.P. Underhill, P.S. Grant, D.J. Bryant and B. Cantor: J Mater. Synthesis and Processing, 1995, vol. 3, pp. 171-179

[15] E. Manson-Whitton, I.C. Stone, J.R. Jones, P.S. Grant and B. Cantor: Acta Mater., 2002, vol. 50, pp. 2517-2535

[16] I.M. Lifshitz and V.V. Slyozov: J. Phys. Chem. Solids, 1961, vol. 19, pp. 35-50

[17] C. Wagner: Z. Elektrochem., 1961, vol. 65, pp. 581-591

[18] P.S. Grant, R.P. Underhill, W.T. Kim, K.P. Mingard and B. Cantor: Proceedings of the Second International Conference on Spray Forming, J.V. Wood (ed.), Osprey Metals, Red Jacket Works, Neath, UK, 1993, pp. 45-54

[19] J.L. Murray and A.J. McAlister: Bulletin of Alloy Phase Diagrams, 1984, vol. 4, pp. 74-90

[20] M. Petrescu: Z. Metallkde., 1970, vol. 61, pp. 14-18

[21] S.C. Hogg: Ph.D. Thesis, University of Sheffield, 2001

[22] S.C. Hogg, C.J.D. Hetherington and H.V. Atkinson: Phil. Mag. Lett., 2000, vol. 80, pp. 477-482

[23] K.A. Jackson: 'Mechanisms of Growth', in Liquid Metals and Solidification, ASM, Cleveland, 1958, p. 174

[24] H.A.H Steen and A. Hellawell: Acta Metall., 1975, vol. 23, pp. 529-535

[25] R-Y Wang, W-H Lu and L.M. Hogan: J. Cryst. Growth, 1999, vol. 207, pp. 43-54

[26] R.S. Wagner: Acta Met., 1960, vol. 8, pp. 57-60

[27] D.R. Hamilton and R.G. Siedensticker: J. Appl. Phys., 1960, vol. 32, pp. 1165-68

[28] C.S. Smith: Trans. Amer. Inst. Min. Met. Eng., 1948, vol. 175, pp. 15-51

[29] V. de L. Davies and J.M. West: J Ins. Met., 1963-64, vol. 92, pp. 175-180

[30] M. Gündüz and J.D. Hunt: Acta Metall., 1985, vol. 33, pp. 1651-1672

[31] P. Keblinski, D. Wolf, S.R. Phillpot and H.J. Gleiter: J Mater. Res., 1998, vol. 13, pp. 2077-2099

[32] P. Keblinski, D. Wolf, S.R. Phillpot and H. Gleiter: Phy. Rev. Lett., 1996, vol. 77, pp. 2965-2968

[33] V. Randle: The Role of the Coincidence Site Lattice in Grain Boundary Engineering, The Institute of Materials, London, 1996

[34] R.J. Jaccodine: J. Electrochemical Soc., 1963, vol. 110, pp. 524-527

[35] J.I. Lee, H.I. Lee and M.I. Kim: Scripta Metall. Mater., 1995, vol. 32, pp. 1945-1949

[36] Y.H. Ryoo, I.J. Kim and K.H. Kim: Proceeding of the Fourth International Conference On The Processing Of Semi-Solid Alloys and Composites, (ed. D.H. Kirkwood and P. Kapranos), The University of Sheffield, Sheffield, England 1996, pp. 66-70

[37] A. Voigt, E. Wolf and H.P. Strunk: Mater. Sci. Eng. B, 1998, vol. B54, pp. 202-206

[38] A. Garg, W.A.T. Clark and J.P. Hirth: Phil. Mag. A, 1989, vol. 59, pp. 1205-1220

Time (mins)	550°C	555°C	558°C	562°C
	f_l	f_l	f_l	f_l
5	0.05	0.06	0.10	0.12
10	0.07	0.10	0.13	0.13
15	0.08	0.09	0.14	0.13
30	0.09	0.11	0.14	0.14
60	0.09	0.09	0.16	0.17
120	0.11	0.13	0.18	0.56
240	0.13	0.15	0.24	0.66
480	0.14	0.30	0.55	0.66

Table 1: Variation of liquid content with time at temperature measured using image analysis.

	Entire Time Range		5-60 Minutes Only	
T (˚C)	Observed coarsening rate constant, K ($m^3 s^{-1}$)	Regression coefficient (R^2)	Coarsening rate constant, K^{5-60} ($m^3 s^{-1}$)	R^2
495	$3.3x10^{-22}$	-	-	-
550	$7.3x10^{-21}$	0.98	$1.5x10^{-20}$	0.98
555	$6.2x10^{-20}$	0.90	$1.4x10^{-20}$	0.86
558	$3.3x10^{-19}$	0.98	$4.4x10^{-20}$	0.98
562	$1.6x10^{-18}$	0.90	$8.4x10^{-20}$	0.99

Table 2: Experimental Coarsening Rate Constants (with Regression Coefficients) for Isothermal Heat Treatments in the Solid State and Semi-Solid State.

D (liquid state – self diffusion of silicon in liquid eutectic Al-Si)	$2.08 \times 10^{-7} \exp(-25732/RT)$ [20]
γ (solid-liquid interface energy)	0.5 Jm^{-2} †
V_m	1.2×10^{-5} m^3/mol

† See section 3.3

Table 3: Data used to predict the coarsening coefficient of silicon particles.

Time (mins)	550°C		555°C		558°C		562°C	
	f_s	Predicted K (m^3s^{-1})	f_s	Predicted K (m^3s^{-1})	f_s	Predicted K (m^3s^{-1})	f_s	Predicted K (m^3s^{-1})
5	0.95	6.7×10^{-17}	0.94	8.2×10^{-17}	0.90	1.4×10^{-16}	0.88	1.7×10^{-16}
10	0.93	9.4×10^{-17}	0.90	1.4×10^{-16}	0.87	1.8×10^{-16}	0.87	1.8×10^{-16}
15	0.92	1.1×10^{-16}	0.91	1.2×10^{-16}	0.86	1.9×10^{-16}	0.87	1.8×10^{-16}
30	0.91	1.2×10^{-16}	0.89	1.5×10^{-16}	0.86	1.9×10^{-16}	0.86	2.0×10^{-16}
60	0.91	1.2×10^{-16}	0.91	1.2×10^{-16}	0.84	2.2×10^{-16}	0.83	2.4×10^{-16}
120	0.89	1.5×10^{-16}	0.87	1.8×10^{-16}	0.82	2.5×10^{-16}	0.44	*1.7×10^{-16}*
240	0.87	1.7×10^{-16}	0.85	2.1×10^{-16}	0.76	3.3×10^{-16}	0.34	*1.2×10^{-16}*
480	0.86	1.9×10^{-16}	0.70	4.1×10^{-16}	0.45	*1.7×10^{-16}*	0.34	*1.2×10^{-16}*
Observed (average)	-	7.3×10^{-21}	-	6.2×10^{-20}	-	3.3×10^{-19}	-	1.6×10^{-18}

Table 4: Solid fraction (f_s) content of the samples, measured by image analysis, and predicted K value as a function of f_s, using equation 3 or 4 (for $f_s < 0.7$ – given in italics). For the purposes of the calculation and to illustrate the effect of f_s we assume that the stated f_s persists for the entire time of the heat-treatment. Included at the bottom of the table are the experimentally observed values for the entire time range.

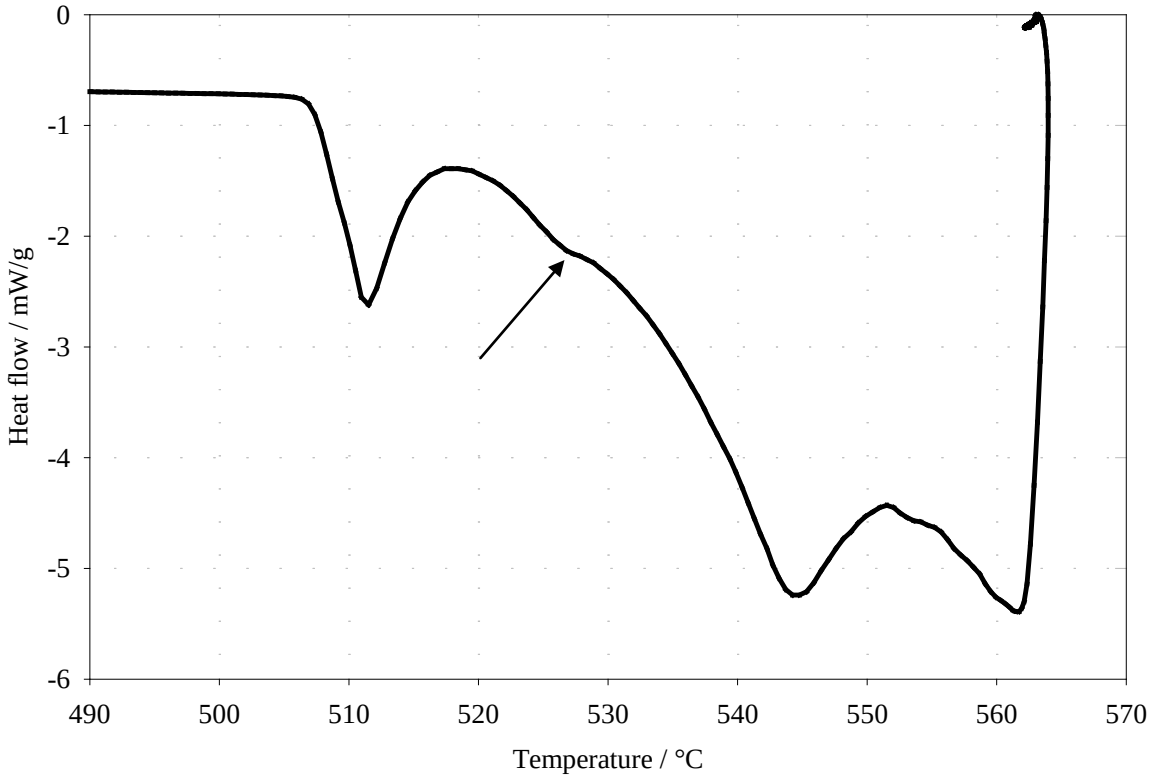

Figure 1: DSC trace obtained on heating to 562°C at 40°C/minute. There are several endotherms indicating eutectic reactions. See text for further details.

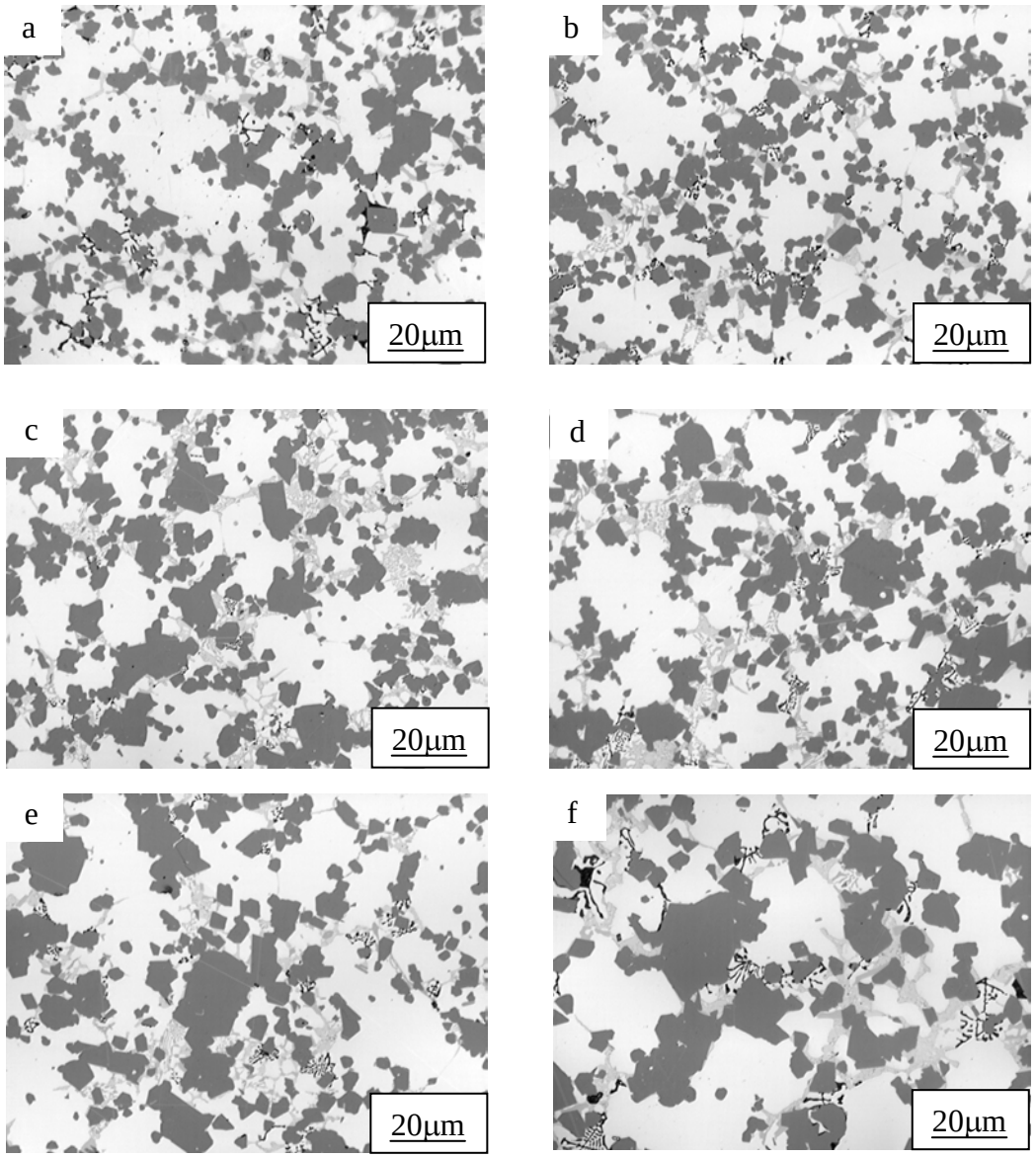

Figure 2: Optical micrographs of the alloy isothermally heat treated at 550°C for (a) 5, (b) 15, (c) 30, (d) 60, (e) 120 and (f) 480 minutes respectively. The lightest phase is the aluminium-solid solution, the dark grey phase is the silicon, and the mid-grey phase is the quenched liquid. Note that the black phase is not an Mg_2Si phase, but probably regions where the quenched liquid has been pulled out during polishing.

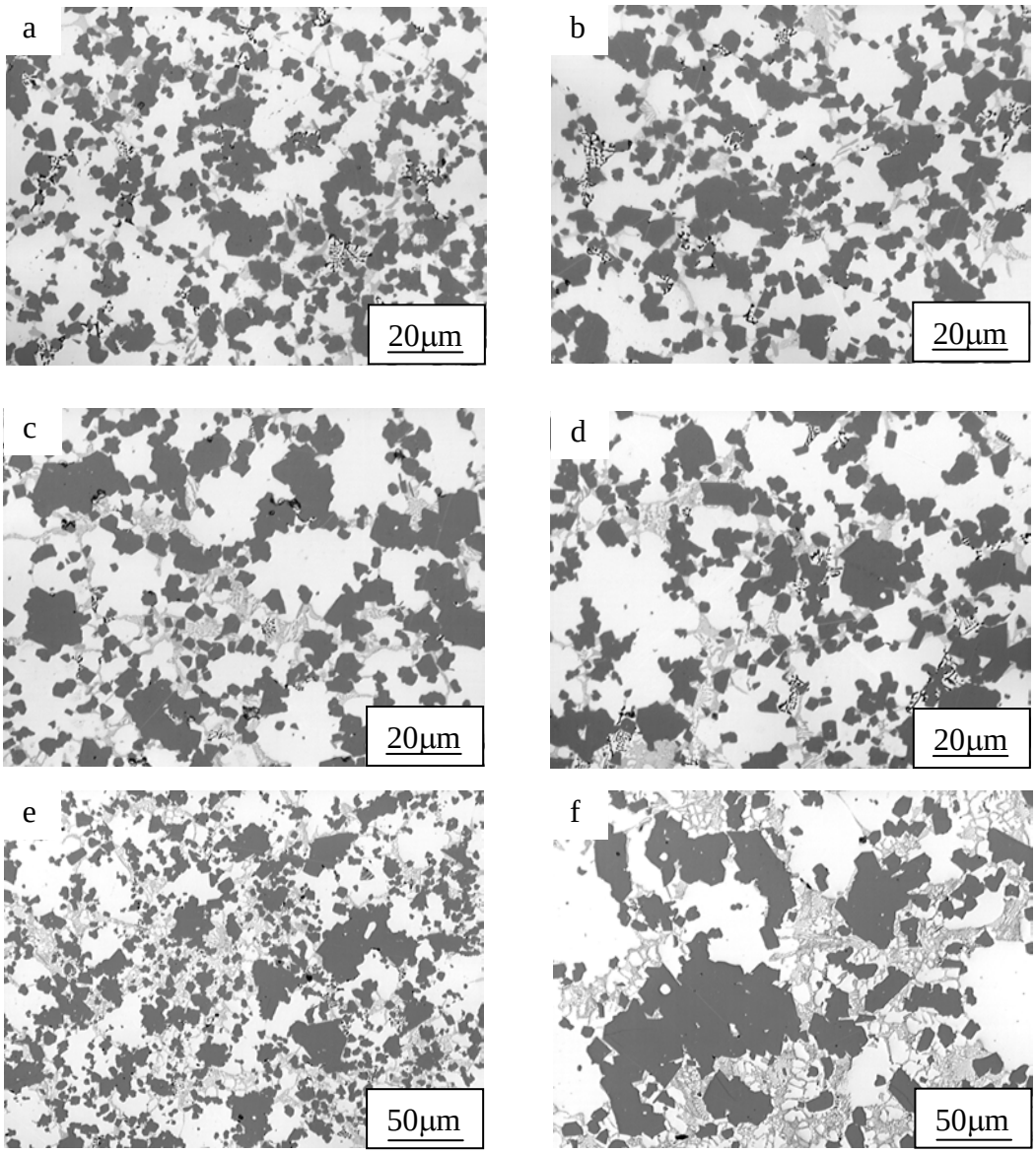

Figure 3: Optical micrographs of the alloy isothermally heat treated at 555°C for (a) 5, (b) 15, (c) 30, (d) 60, (e) 120 and (f) 480 minutes respectively.

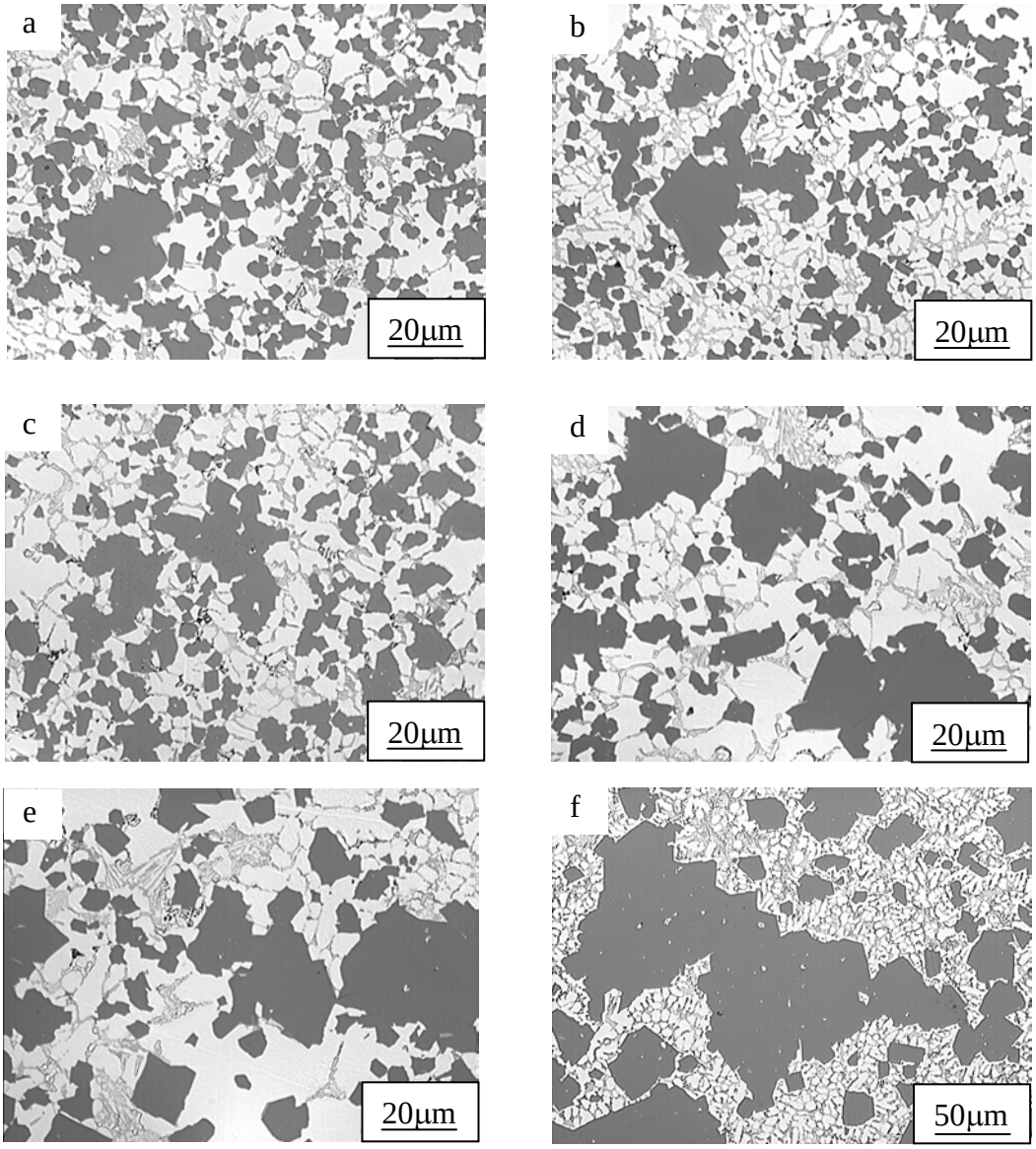

Figure 4: Optical micrographs of the alloy isothermally heat treated at 558°C for (a) 5, (b) 15, (c) 30, (d) 60, (e) 120 and (f) 480 minutes respectively.

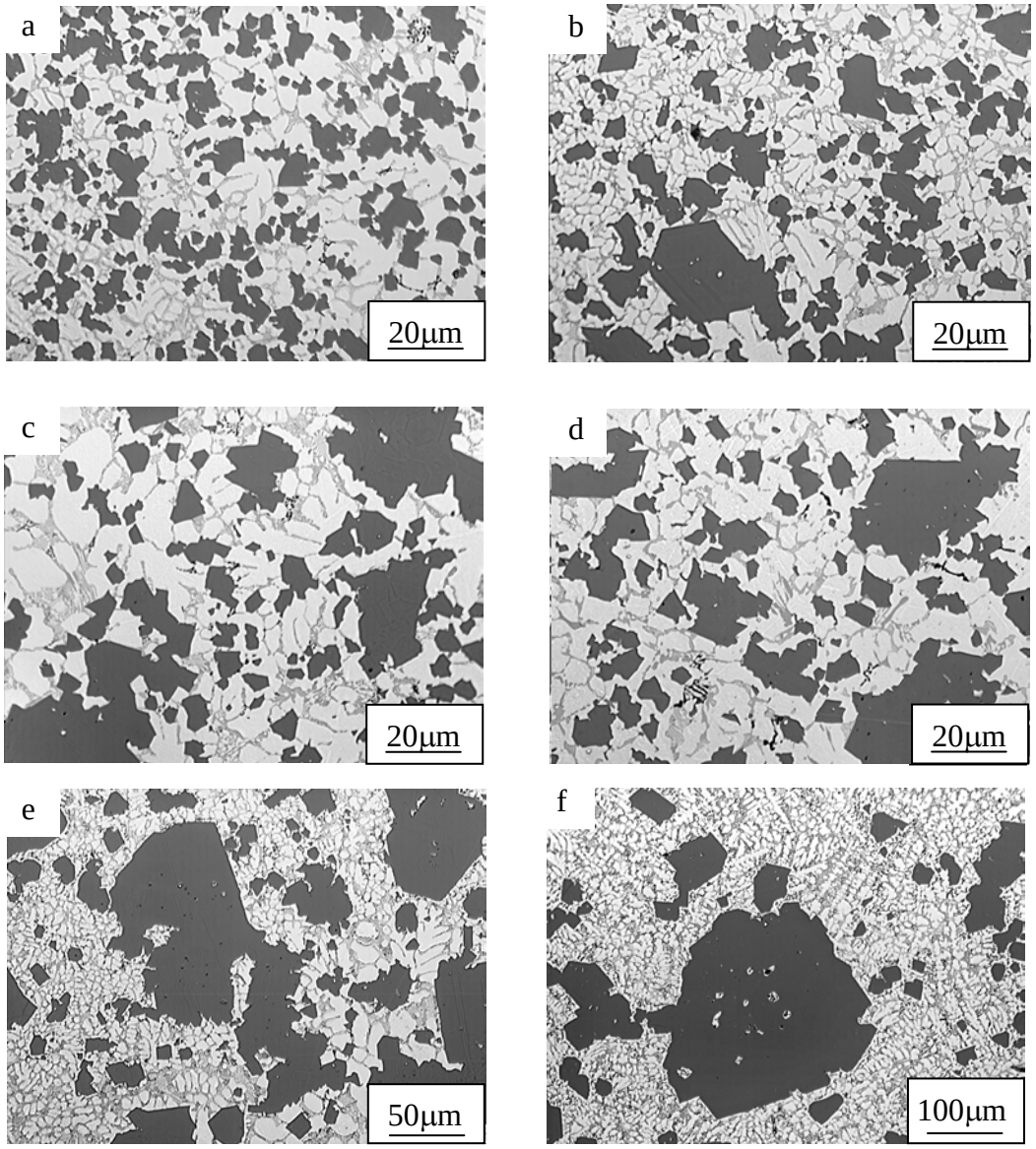

Figure 5: Optical micrographs of the alloy isothermally heat treated at 562°C for (a) 5, (b) 15, (c) 30, (d) 60, (e) 120 and (f) 480 minutes respectively.

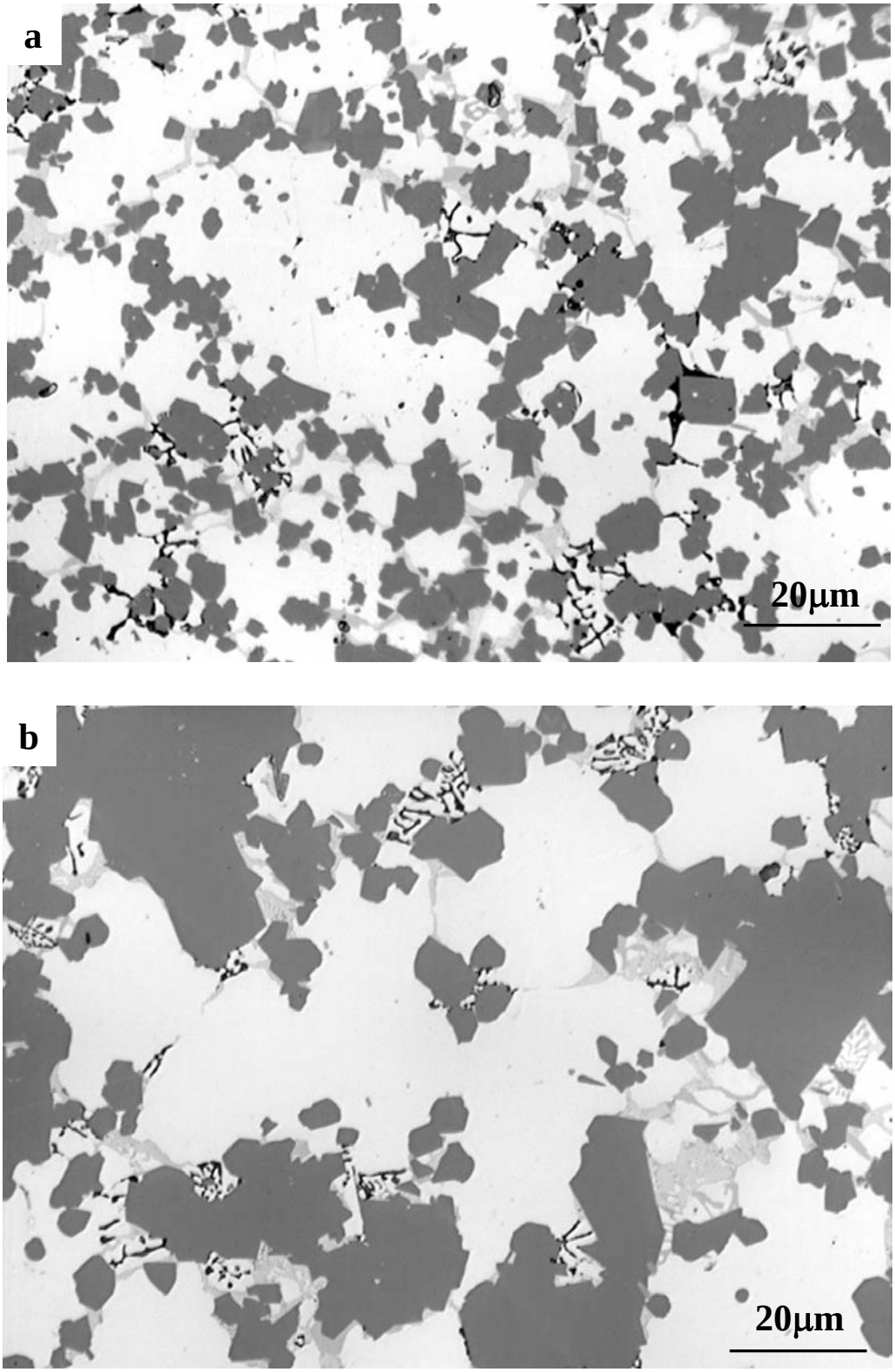

Figure 6 (a) and (b): Optical micrographs of the alloy isothermally heat treated at 550°C for 5 minutes and 8 hours respectively. The liquid content is initially low and increases only slightly even after 8 hrs. Again, as in figure 1, note that the black phase is not an Mg_2Si phase, but probably regions where the quenched liquid has been pulled out during polishing.

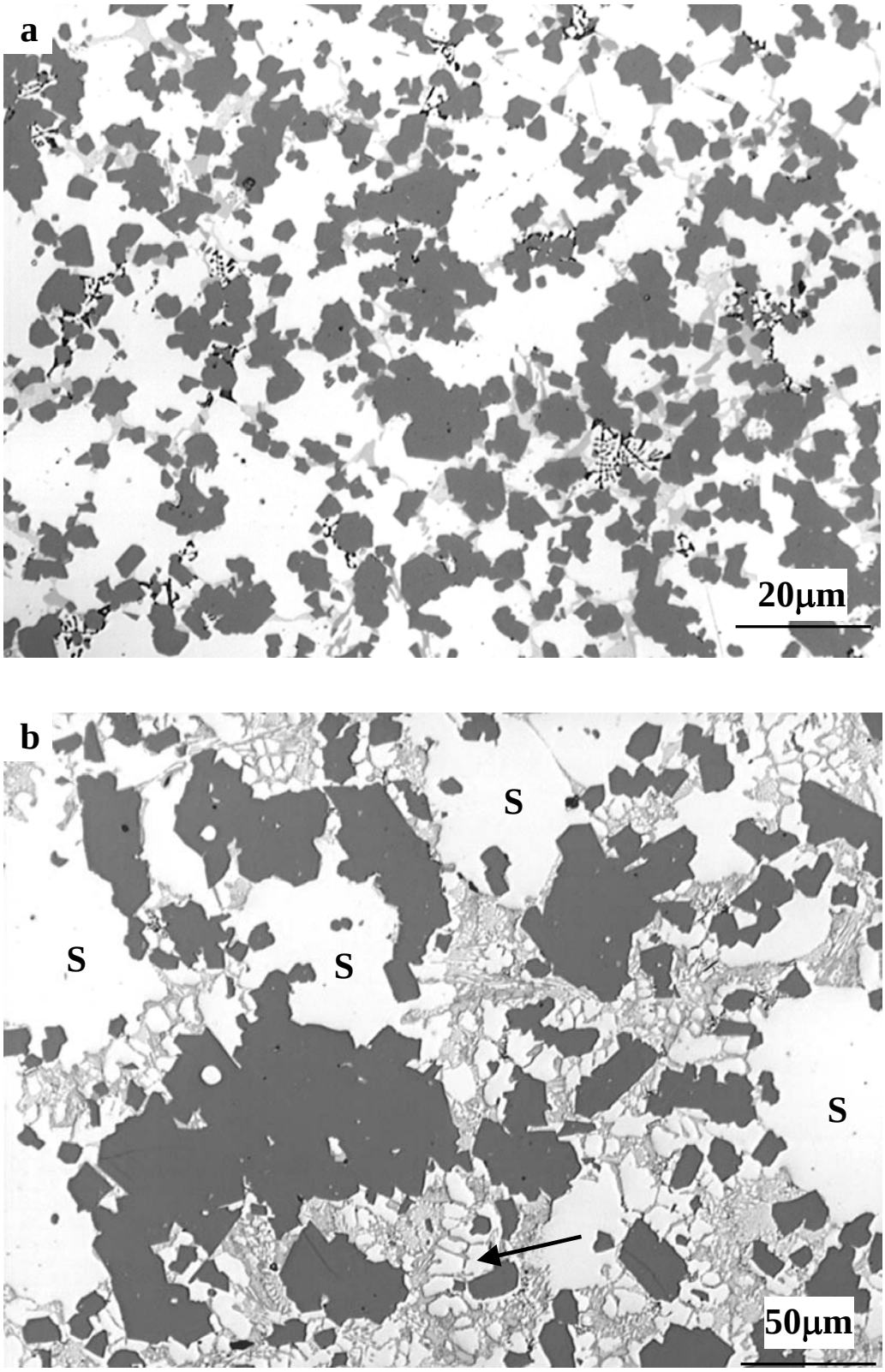

Figure 7 (a) and (b): Microstructures after isothermal heat treatment at 555°C for 5 minutes and 480 minutes respectively. The observed liquid contents vary significantly with time at temperature. There is dendritic aluminium from quenched liquid in (b) (arrowed), but some aluminium spheroids still remain (labelled 'S').

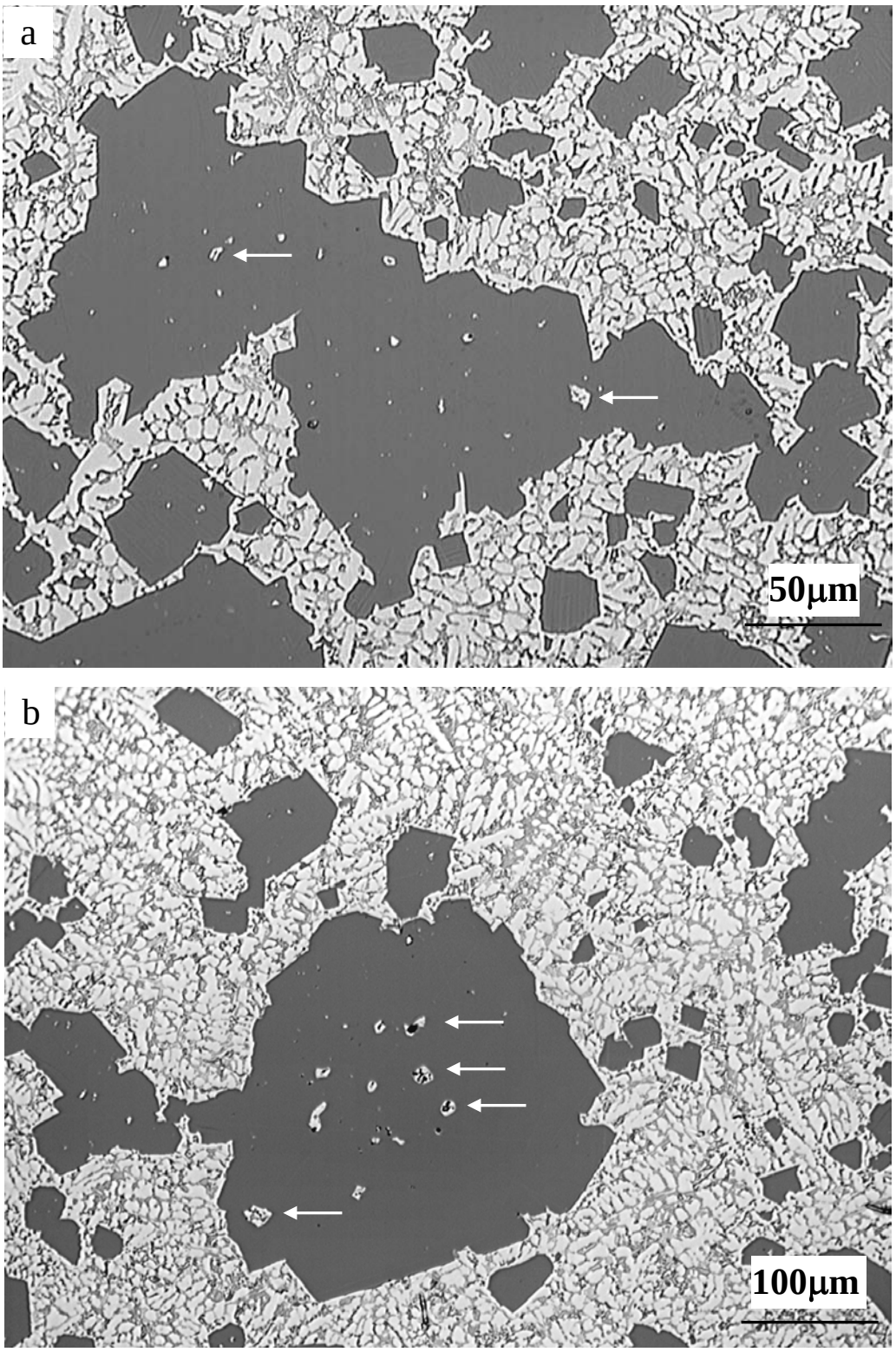

Figure 8 (a) and (b): Observed microstructure of the alloys isothermally heat treated for 8 hours at 558°C and 562 °C respectively. The microstructure consists of silicon + quenched liquid. Note the large amount of entrapped liquid within the large silicon grains in (a) and (b). Examples are arrowed. Note also the 'branched' or clustered silicon morphology.

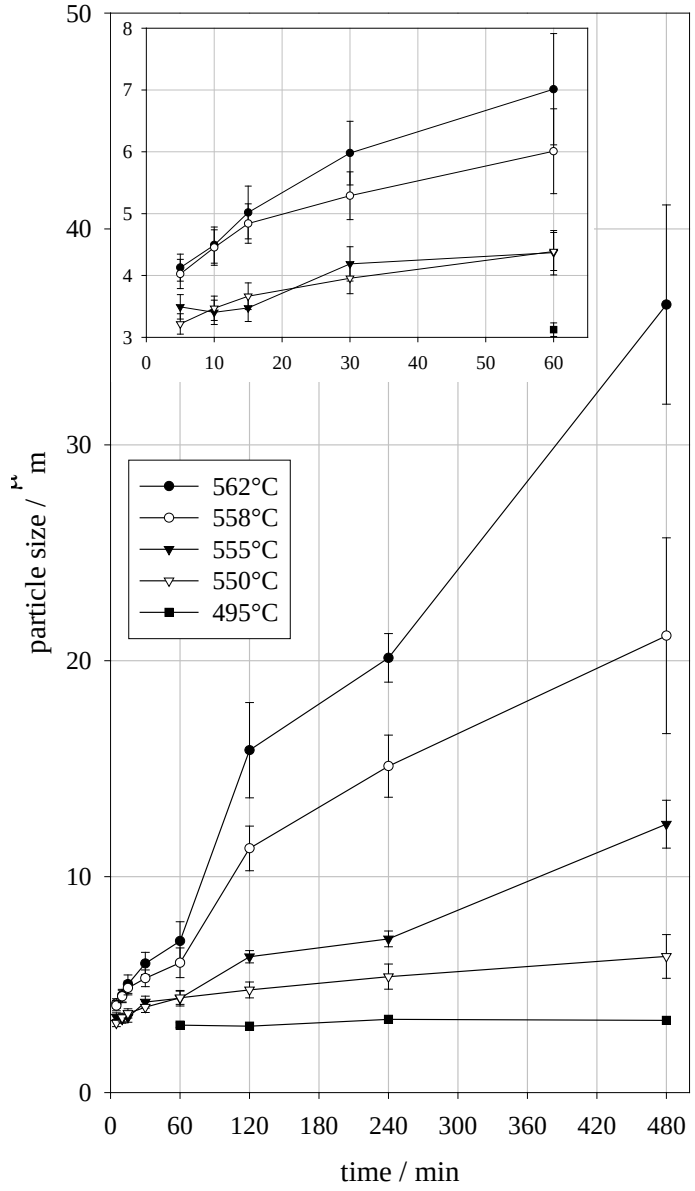

Figure 9: Average silicon particle size as a function of time at temperature. The insert is a magnification of the 5 – 60 minutes coarsening time. Error bars indicate the 95% confidence limits (±).

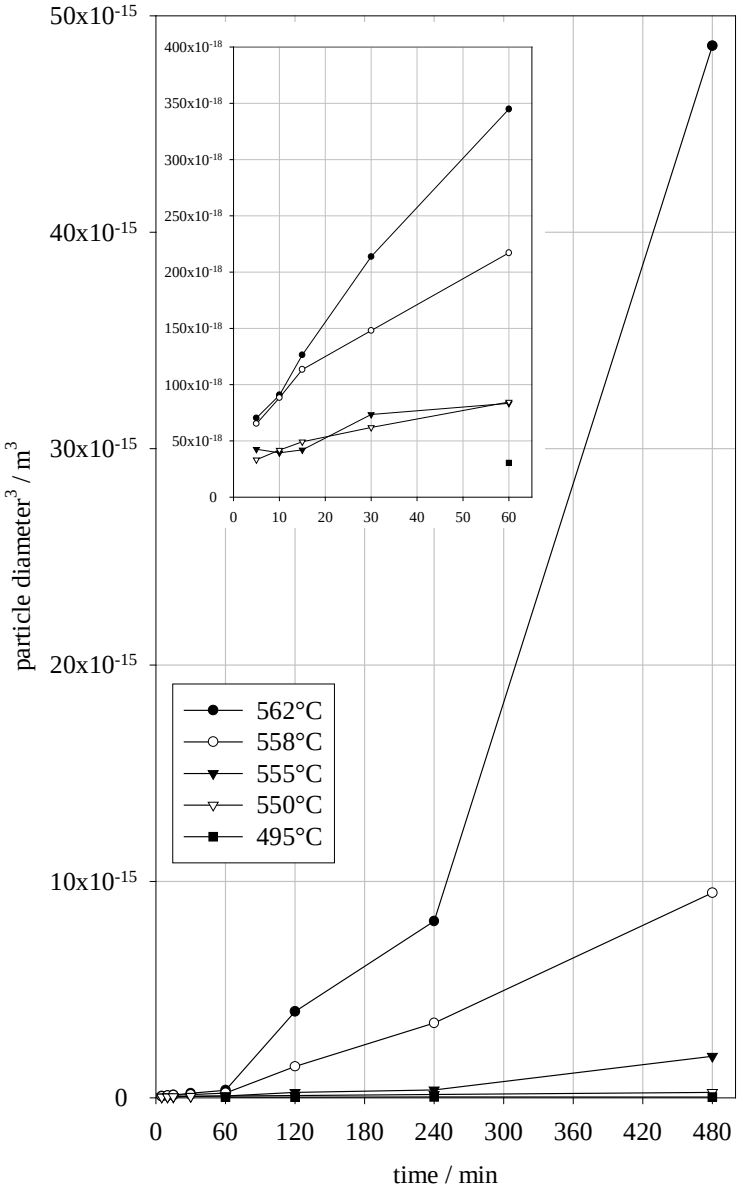

Figure 10: Average silicon particle size cubed as a function of time at temperature. The insert is a magnification of the 5 – 60 minutes coarsening time.

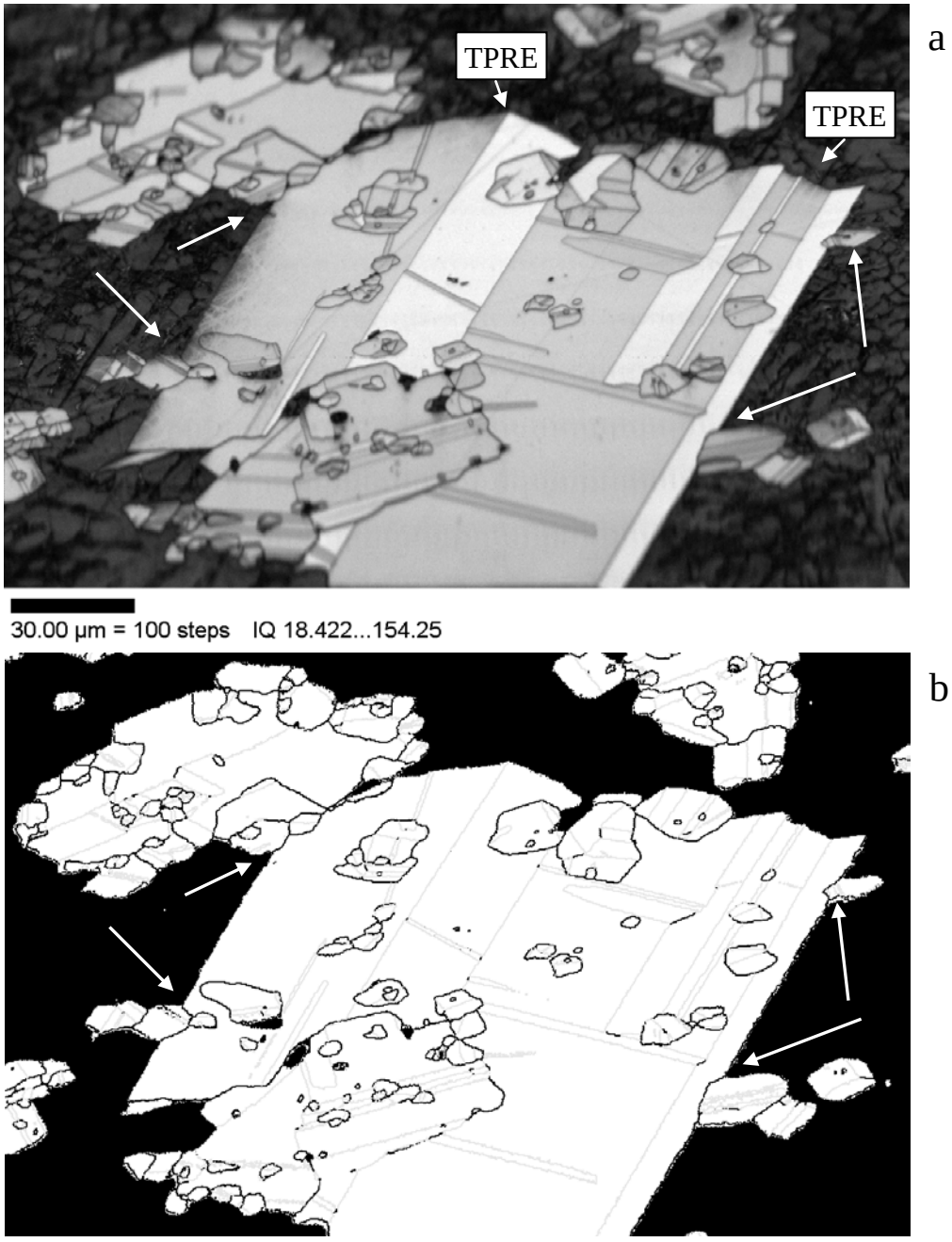

Figure 11: (a) EBSD image pattern quality map and (b) EDS partitioned black and white map (silicon regions are white) showing high angle (>15°) boundaries in black, and 59-61° boundaries, corresponding to Σ3 {111} twin boundaries, in grey. Grains have attached to the {111} facets of the large central grain (arrowed). Also evident are twin grooves and ledges, indicating the twin plane re-entrant (TPRE) mechanism is contributing to silicon growth (labelled in (a) as TPRE).